Optical investigation of a τ-phase organic molecular conductor: τ-(EDO-(S,S)-DMEDT-TTF)$_2$(AuBr$_2$)(AuBr$_2$)$_y$ ($y\approx0.75$)

I. Olejniczak* and J. L. Musfeldt
Department of Chemistry, State University of New York at Binghamton, Binghamton, New York 13902-6016

G. C. Papavassiliou and G. A. Mousdis
Theoretical and Physical Chemistry Institute, National Hellenic Research Foundation, Athens 116/35, Greece
(Received 29 June 1999; revised manuscript received 23 August 2000)

We report the infrared and optical properties of a quasi-two-dimensional organic conductor τ-(EDO-(S,S)-DMEDT-TTF)$_2$(AuBr$_2$)(AuBr$_2$)$_y$ ($y\approx0.75$), where EDO-(S,S)-DMEDT-TTF is ethylenedioxy-(S,S)-dimethylethylene-dithio-tetrathiafulvalene, as a function of temperature. This cation radical salt, based on an unsymmetrical π donor, displays an unusual temperature dependence of the low-lying electronic excitation, attributed to electronic localization effects. The two components of the low-lying electronic structure were studied by standard fitting procedures and show different behavior with temperature, suggesting that they may steal oscillator strength from a narrow Drude feature. The trends are interpreted within the Hubbard model. Vibrational CH_2-related features show also signs of disorder, suggesting a connection with the electronic localization and a proposed magnetic phase transition at low temperature.

I. INTRODUCTION

Recently, there has been a great deal of interest in organic molecular solids based upon symmetrical and asymmetric donor building block molecules.[1–8] This is because of their interesting physical properties, e.g., high conductivity or superconductivity, novel magnetic phases, and the possibility to study the effect of chemical structure on the physical properties. Among the prototype materials are the salts crystallized in the α, β, θ, λ, and κ phases. Bis(ethylenedithiolo)tetrathiafulvalene (ET)-based single crystals of the κ type, which are characterized by layers of orthogonal mixed-valence dimers, exhibit the highest superconducting transition temperatures of quasi-one- and two-dimensional organic layered superconductors.[9–11] At the same time, it was discovered that some salts with linear anions (X) based on unsymmetrical tetrachalcogenafulvalene donor molecules (D), are crystallized in a tetragonal system, the so-called τ-phase of the formula τ-(D)$_2$(X)$_1$(X)$_y$ (where X=I$_3$,IBr$_2$,AuBr$_2$, AuI$_2$).[12,13] In this phase, mixed cation–anion layers alternate with anion layers, and the resulting crystals are metallic in directions parallel to the layers (i.e., in the ab plane). Most of the research in this area is focused on the salts of chiral donor molecules P-(S,S)-DMEDT-TTF and EDO-(S,S)-DMEDT-TTF; examples are the organic metal τ-(P-(S,S)-DMEDT-TTF)$_2$(AuBr$_2$)(AuBr$_2$)$_y$ and the semiconductor τ-(EDO-(S,S)-DMEDT-TTF)$_2$(I$_3$)(I$_3$)$_y$ with $y\approx0.75$.[14,15] It is the rather unusual τ-phase which is of interest here.

The salt based on ethylenedioxy-S,S- dimethylene-dithiotetrathiafulvalene (abbreviated as EDO-S,S-DMEDT-TTF) in combination with linear anion AuBr$_2$ is a model τ-phase solid.[13] Each unit cell of τ-(EDO-(S,S)-DMEDT-TTF)$_2$(AuBr$_2$)(AuBr$_2$)$_y$ (with $y\approx0.75$) contains eight donor molecules D^{n+} [where $n=(1+y)/2$], which are orthogonally arranged with the long axis parallel to the c direction, forming a two-dimensional (2D) network in ab plane. There are S$\cdots$S and S$\cdots$O contacts, which are smaller than or close to the sum of the corresponding van der Waals radii. Four counter anions ($AuBr_2^-$) occupy well-defined lattice sites in the conducting 2D layer (Fig. 1), and four $(AuBr_2^-)_y$ are disordered along the b-axis at $a=0$ and $c=0.125$ between conducting layers.[16] Another source of disorder is the ethylenedioxy groups.

A remarkable feature of this material is that y is not an integer, and therefore it strongly influences the material properties. The Fermi surface (FS) of τ-(EDO-(S,S)-DMEDT-TTF)$_2$(AuBr$_2$)(AuBr$_2$)$_y$ is star shaped.[16]

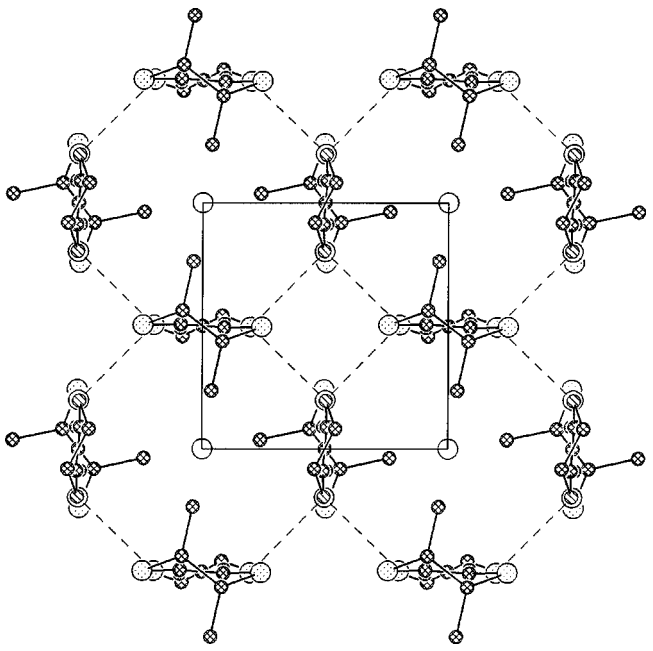

FIG. 1. Molecular organization of a conducting layer (ab plane) in τ-(EDO-(S,S)-DMEDT-TTF)$_2$(AuBr$_2$)(AuBr$_2$)$_y$ seen along the longest molecular axis (dashed lines indicate the S–S and S–O intermolecular contacts).

According to electronic band structure calculations, smaller values of y result in larger FS areas; even within the 2D plane, a weak fourfold anisotropy is expected.[17] Within the calculated band structure, one predicts interband transitions at ≈ 1500 and $\approx 3900\,\mathrm{cm}^{-1}$. The calculated charge transfer integrals (t) in the ab plane are almost 10 times larger for perpendicular molecules than for parallel ones. The τ-(EDO-(S,S)-DMEDT-TTF)$_2$(AuBr$_2$)(AuBr$_2$)$_y$ salt displays strong anisotropy in the in-plane vs out-of-plane DC conductivity ($>10^3$).[16] The metal-like resistivity, which shows no anisotropy in the ab plane itself, is almost logarithmically decreasing with decreasing temperature, although it displays an upturn at low temperature;[16] the in-plane conductivity σ_{DC} is ≈ 50 and $\approx 550\,\Omega^{-1}\,\mathrm{cm}^{-1}$ at 300 and 10 K, respectively. Possible ionic conductivity effects are thought to complicate these measurements,[18] and the main effect is to enlarge the total value of conductivity. The Hall coefficient shows a negative value below 150 K,[16] indicative of negatively charged carriers in agreement with the electron band structure calculations, and variation of the scattering path length over the FS.[19] The low-field magnetoresistance is negative in the insulating region,[15,16] and its magnitude increases with decreasing temperature. No magnetic oscillations were observed, indicative of an open FS. For high applied fields, the 2.1 K magnetoresistance becomes positive. This suggests a 2D weak-localization effect and possible metal$\rightarrow$insulator transition below 10 K.[20] Further, in the low temperature state, the magnetoresistance exhibits a hysteretic behavior during the field cycle which suggests the presence of a correlated magnetic state.[15] Recently, the symmetry of the angle-dependent magnetoresistance was found to be fourfold or twofold, depending on the temperature and magnetic field,[17] which was discussed in terms of weak ferromagnetism and formation of magnetic domains.[21] Previous room temperature spectral studies in this material[18] identified electronic charge transfer bands centered near 1500, 5500, and $11\,000\,\mathrm{cm}^{-1}$, together with vibrational features in the middle infrared region. Because of the low symmetry of the donor molecule, the characteristic broad totally symmetric vibronic modes which dominate the spectra of many organic solids with symmetrical donor molecules are absent. A few modes were assigned as C=C or CCS/CCO vibrations of the donor molecule. No spectral anisotropy was found in the ab plane. Raman scattering and middle infrared studies have also been used to characterize the 300 K spectra of the donor isolated molecule.[18]

In order to provide further information on the nature of charge localization and disorder in τ-phase organic solids, we have investigated the infrared and optical properties of τ-(EDO-(S,S)-DMEDT-TTF)$_2$(AuBr$_2$)(AuBr$_2$)$_y$ as a function of temperature. Our overall goal is to identify electronic processes which may be important for stabilizing the low-temperature localized state in this material, and vibrational features serving as a probe of its existence.

II. EXPERIMENTAL

Crystals of τ-(EDO-(S,S)-DMEDT-TTF)$_2$(AuBr$_2$)$\times$(AuBr$_2$)$_y$ were obtained by electro-oxidation of the donor[16] as dark, reflecting platelets with typical dimensions of $1\times1\times0.02\ \mathrm{mm}^3$. The salt is crystallized in a tetragonal system, space group $I4_122$ with $a=b=7.4048$ Å, $c=67.995$ Å, and $V=3728.23\ \mathrm{Å}^3$. We were unable to confirm the previously reported ESR signal at room temperature.[16]

Near normal reflectance measurements of a single crystal sample of τ-(EDO-(S,S)-DMEDT-TTF)$_2$(AuBr$_2$)(AuBr$_2$)$_y$ were made with a Bruker 113V Fourier transform spectrometer ($30-5000\,\mathrm{cm}^{-1}$) and a Perkin-Elmer Lambda-900 grating spectrometer ($4000-40\,000\,\mathrm{cm}^{-1}$). For the far-infrared (FIR) measurements, a helium cooled bolometer detector was used to obtain an enhanced sensitivity. Traditional room temperature detectors were employed over the middle and near infrared (MIR, NIR), optical, and ultraviolet (UV) ranges. The transmission spectra of powdered salt dispersed in a KBr pellet were measured using the Bruker 113V ($450-5000\,\mathrm{cm}^{-1}$) as well.

Infrared and optical measurements were made at several temperatures in reflectance mode: 300, 200, 100, and 15 K. In transmission, only 300 and 15 K data were collected. For temperature control, we used an open-flow cryostat mounted in the reflectance (or transmission) stage of the spectrometer. An aluminum mirror was used as a reference, and an overcoat of aluminum was used to estimate scattering losses. We searched for optic axes on the large crystal face (ab) parallel to conducting layers, but no polarization dependence was found over the entire frequency range measured here, in agreement with previous work.[18] Based upon the crystal structure, this is the expected result.

A Kramers–Kronig analysis of the reflectance data was performed to obtain the real and imaginary parts of the dielectric function, and thus the optical constants of each material $[\sigma_1(\omega),\epsilon_1(\omega),N_{\mathrm{eff}}(m/m^*)]$.[22] Note that ϵ_1 is the real (in-phase) part of the dielectric function and σ_1 is the imaginary, out-of-phase part. The high frequency extrapolation to the Kramers–Kronig phase integral was done as $\omega^{-1.5}$, and the low frequency extrapolation with a metallic Hagen–Rubens-type extrapolation, which is appropriate for this conducting salt. Small level differences often result from using a limited frequency range in a Kramers–Kronig analysis, as we estimated using different low frequency extrapolations. The available structural data were used to extract the effective mass from the sum rule information. Absorption was calculated from transmission as $A(\omega)=-(1/hd)\ln T(\omega)$, where h is the sample loading in the KBr matrix, and d is the pellet thickness.

Standard PEAKFIT procedures were used for fitting the frequency dependent conductivity data. A variety of line shapes were tested for suitability, including Lorenzian, Voigt, asymmetric double Gaussian cumulative, and asymmetric double sigmoidal. All the applied functions were modified Lorenzians or Gaussians. Overall, Voigt and asymmetric Gaussian gave the most satisfactory results for the first and second components, respectively. Errors were estimated statistically based upon the results obtained for slightly different fitting procedures involving different spectral functions and reasonable background choices.

III. RESULTS

Figure 2 displays the temperature dependence of the near-normal reflectance of τ-(EDO-(S,S)-DMEDT-

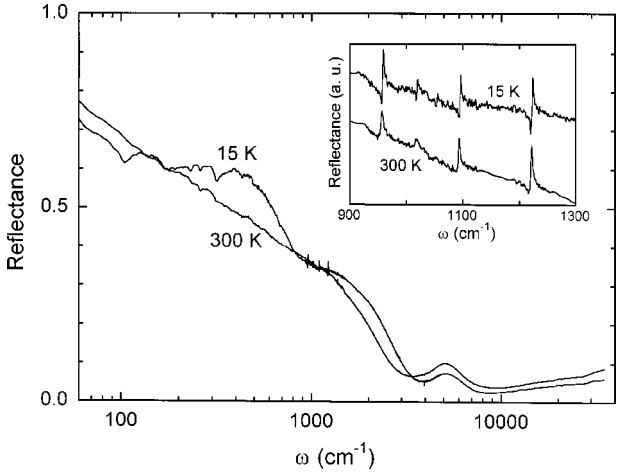

FIG. 2. Unpolarized reflectance of τ-(EDO-(S,S)-DMEDT-TTF)$_2$(AuBr$_2$)(AuBr$_2$)$_y$ in the ab plane, at 300 and 15 K. The inset displays a close-up view of the MIR vibrational features. Note the logarithmic frequency scale in the main panel.

TTF)$_2$(AuBr$_2$)(AuBr$_2$)$_y$ in the conducting ab plane. The overall response is that of an isotropic two-dimensional conductor, with high reflectance in the FIR. However, the spectra do not show a well-defined plasma edge and associated reflectance minimum characteristic of a Drude ''free electron'' metal. The overall reflectance level is slightly higher at 15 K, and a low-lying electronic structure in the MIR shows strong temperature dependence. The vibrational features, superimposed on the electronic structure, are screened as is often observed in highly conducting organic materials but clearly visible in the MIR. The inset of Fig. 2 displays the weak temperature dependence of the MIR vibrational features.

Figure 3 shows the frequency dependent conductivity of

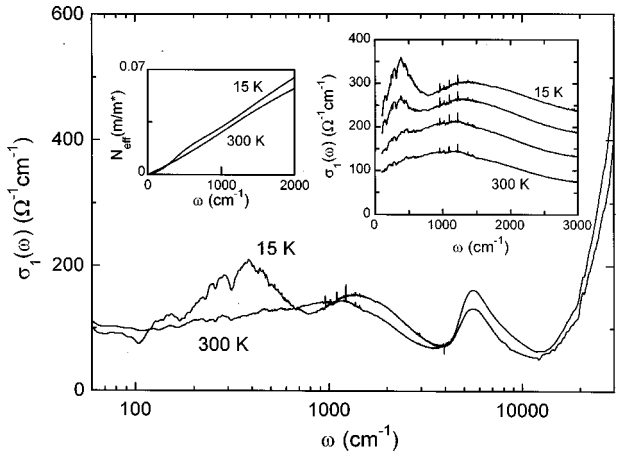

FIG. 3. Frequency dependent conductivity of τ-(EDO-(S,S)-DMEDT-TTF)$_2$(AuBr$_2$)(AuBr$_2$)$_y$ as a function of temperature in the ab plane; 300 and 15 K data are shown in the main plot. Right inset: a close-up view of the doublet structure in the low-lying electronic band; from top to bottom, temperatures are: 15, 100, 200, and 300 K; 15, 100 and 200 K spectra are offset from the 300 K curve for clarity by 150, 100 and 50 Ω^{-1}cm^{-1}, respectively. Left inset: conductivity sum rule for τ-(EDO-(S,S)-DMEDT-TTF)$_2$(AuBr$_2$)(AuBr$_2$)$_y$ at 300 and 15 K.

τ-(EDO-(S,S)-DMEDT-TTF)$_2$(AuBr$_2$)(AuBr$_2$)$_y$ as a function of temperature. The spectra are dominated by several broad electronic features. In the 300 K spectrum, one structure is centered at $\approx$5500 cm^{-1}, and a second very broad and somewhat asymmetric band is observed near 1000 cm^{-1}. It is the low-lying electronic excitation at 1000 cm^{-1}, which shows a distinct splitting at reduced temperature, that is of primary interest. The trend with temperature is more clearly visible in the right-hand inset of Fig. 3. At room temperature, two oscillators (centered at $\approx$350 and $\approx$1100 cm^{-1}) are needed for the model oscillator fit. That two oscillators are appropriate (and essential) to mimic this structure becomes more obvious as temperature is lowered. The doublet structure is also visible on the plot of the partial sum rule of the conductivity (left-hand inset of Fig. 3) which relates the oscillator strength to the effective mass and the effective number of carriers per formula unit participating in optical transitions. Assuming a carrier concentration resulting from seven carriers per unit cell, we find $m^* \approx 6.7 m_e$. As expected from the reflectance, there is no zero crossing in the frequency dependent dielectric constant, $\epsilon_1(\omega)$ (not shown). Extrapolation of $\sigma_1(\omega)$ to zero frequency gives lower DC conductivity than that predicted by transport results, indicating the likely influence of low-frequency free carrier contribution (and the associated oscillator strength) below the limit of our measurements combined with effects of ionic conductivity. Such a narrow Drude feature has been speculated in a number of organic solids.[23,24]

The temperature dependence of the low-lying electronic excitation was analyzed using fitting procedures. Following the assumption of doublet structure, we have fit the experimental data with two spectral functions. Figure 4 displays the temperature dependence of the band parameters that result from our fit. The parameters highlight quite different behavior for the two components. Most of the oscillator strength of the excitation is due to the broad higher energy band (centered at $\approx$1100 cm^{-1} at 300 K). The center frequency of this component is strongly temperature dependent, reaching a value of $\approx$1380 cm^{-1} at 15 K, whereas the frequency of the narrow component at $\approx$350 cm^{-1} is temperature independent. Taking into account errors of the fitting procedure, the oscillator strength of the broad component is almost temperature independent; on the other hand, the narrow band at $\approx$350 cm^{-1} is hardly noticeable at 300 K but its oscillator strength quickly grows with decreasing temperature. Both components show the usual linewidth narrowing at low temperature. Within our resolution, all the band parameters show monotonic behavior and no anomaly was found around the possible 50 K phase transition temperature. However, the fit results allow us to conclude that the temperature dependence of the low-lying electronic doublet structure is complicated, and can be connected with different types of excitation for the broad and narrow components. Extension of these measurements to lower energy would likely confirm the shifting of oscillator strength from a narrow Drude to the far infrared. The relative strength of the narrow low-energy oscillator can be related to the degree of localization, as discussed below.

This well-pronounced splitting of the electronic structure is supported by the data in the lower panel of Fig. 5, showing the 15 K absorption spectrum of τ-(EDO-(S,S)-

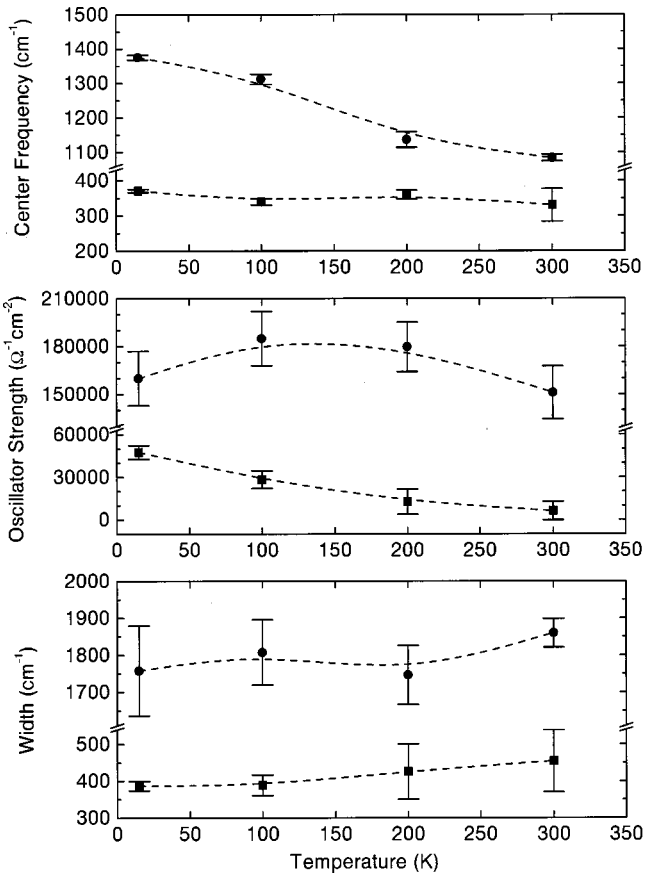

FIG. 4. Temperature dependence of the fit parameters describing the low-lying electronic doublet structure of τ-(EDO-(S,S)-DMEDT-TTF)$_2$(AuBr$_2$)(AuBr$_2$)$_y$. Solid circles: higher frequency component at $\approx$1100 cm^{-1}, solid squares: lower frequency component at $\approx$350 cm^{-1}. Determination of the error bars is described in the text. Lines are intended to guide the eye.

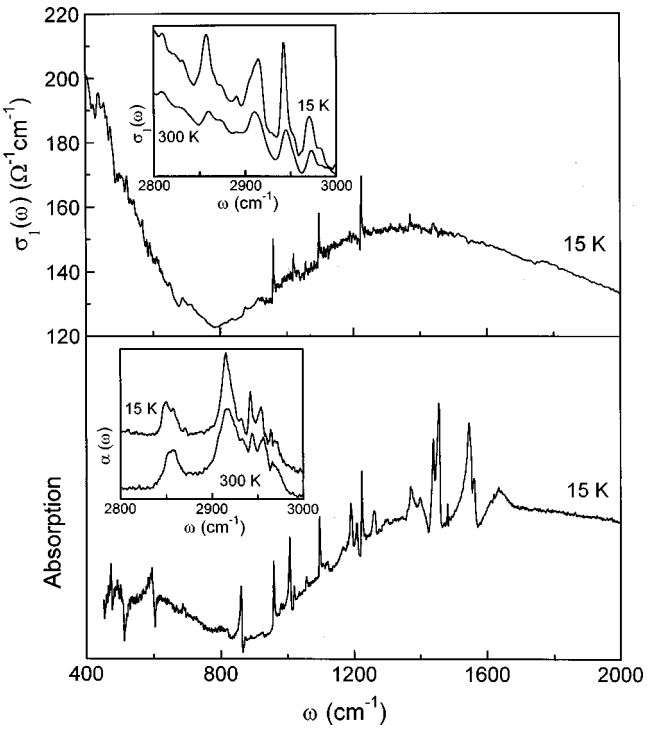

FIG. 5. Upper panel: frequency dependent conductivity of τ-(EDO-(S,S)-DMEDT-TTF)$_2$(AuBr$_2$)(AuBr$_2$)$_y$ at 15 K in the ab plane, obtained by Kramers-Kronig transform of the reflectance. Lower panel: 15 K absorption spectrum of τ-(EDO-(S,S)-DMEDT-TTF)$_2$(AuBr$_2$)(AuBr$_2$)$_y$, obtained from the transmission spectrum. The upper inset displays a close-up view of the conductivity in the range of CH_2 vibrations, at 300 and 15 K. The lower inset displays a close-up view of the absorption in the range of CH_2 vibrations, at 300 and 15 K. Note that data in the top panel is from the ab plane of a single crystal sample, whereas data in the lower panel is that from an isotropic (KBr pellet) sample.

DMEDT-TTF)$_2$(AuBr$_2$)(AuBr$_2$)$_y$ taken in transmission mode. Thus, the doublet structure centered between 300 and 1400 cm^{-1} is observed by two independent measurements. Furthermore, the transmission data reveal a large number of vibrational features previously assigned to the donor molecule.[18] Only a few of these modes are visible in the 15 K frequency dependent conductivity (upper panel of Fig. 5), as one might expect for a spectrum taken in the ab plane of a single crystal. For instance, in the 400–2000 cm^{-1} regime, only four modes (near 950, 1020, 1090, and 1225 cm^{-1}) are preferentially polarized in the conducting ab plane. On the other hand, in the CH_2 region, most modes are preferentially in-plane, except the small shoulder near 2935 cm^{-1} and the feature at $\approx$2955 cm^{-1}. Modest temperature dependence was observed in the range of CH_2 vibrations, as shown in the upper (conductivity) and lower (absorption) insets of Fig. 5. Here, the 2860 and 2945 cm^{-1} modes seem most different; other vibrational features show the usual narrowing at low temperature, due to reduced damping.

IV. DISCUSSION

A. Electronic spectra

The most striking feature of the optical conductivity of τ-(EDO-(S,S)-DMEDT-TTF)$_2$(AuBr$_2$)(AuBr$_2$)$_y$ is the low-temperature splitting of the electronic excitation centered near 1000 cm^{-1} (Figs. 3 and 5) into two components; these oscillators are at $\approx$350 and $\approx$1100 cm^{-1} at 300 K. Based on the optical studies of BEDT-TTF and BEDO-TTF materials, one could relate this band as well as the high frequency structure centered at $\approx$5500 cm^{-1} to interband excitations.[18,25,26] The attractive aspect of this picture is that we can assign the electronic features using existing room temperature band structure calculations[16] which suggest the presence of interband transitions at $\approx$1500 and $\approx$3900 cm^{-1}; microscopic assignments of excitations follow readily as well, in reasonable agreement with our data. Then, the pronounced band splitting observed at reduced temperature should be connected with a distortion of the unit cell influencing the band structure. However, the doublet structure in the spectra develops over a broad temperature range starting from room temperature and does not seem to be connected with a specific phase transition (Fig. 4). Further, no appreciable structural change was observed at low temperatures in x-ray studies.[17] Therefore, we conclude that band structure calculations do not offer a way to account for the changing electronic localization in τ-(EDO-(S,S)-DMEDT-TTF)$_2$(AuBr$_2$)(AuBr$_2$)$_y$.

On the other hand, $m^* \approx 6.7 m_e$ was extracted from the partial sum rule on the frequency dependent conductivity.

Hence, taking into account the existence of a highly correlated state, other theoretical approaches based upon the Hubbard model[27–29] may also be suitable for describing the broad low-lying electronic structure in the conductivity spectrum of τ-(EDO-(S,S)-DMEDT-TTF)$_2$($AuBr_2$)($AuBr_2$)$_y$. Indeed, the optical properties of a number of materials, including $(TMTSF)_2PF_6$ and β''-$(ET)_2SF_5CH_2CF_2SO_3$ are not readily described by Fermi liquid theory.[30,31] Within the basic Hubbard framework, the low-temperature optical spectrum is predicted to show a Drude-type signature centered at zero frequency due to quasiparticle transitions, a resonance at $\omega \approx U/2$ (U is the on-site Coulomb repulsion) due to transitions between the Hubbard bands and the quasiparticle band, and a contribution at $\omega \approx U$ which appears due to transitions between lower and upper Hubbard bands.[32] Within this picture, the band centered at $\approx 5500\,cm^{-1}$ in τ-(EDO-(S,S)-DMEDT-TTF)$_2$($AuBr_2$)($AuBr_2$)$_y$ is then due to charge transfer transitions between the lower and upper Hubbard bands. Consequently, the excitation at $\omega \approx U/2$ may account for the low-lying doublet structure. Other models,[33,34] which include both on-site (U) and near-neighbor (V) interactions, explain different ways to consider perturbations to this gap. As the Hubbard picture is a localized one, we assign the low frequency part of the doublet structure (the low-energy oscillator) that grows with decreasing temperature as being related to additional low-temperature charge localization. Similar doublet character in the electronic structure has also been observed in other materials and attributed to the interdimer charge transfer in the presence of strong dimerization.[35] Although no distinct free carrier component is found down to 15 K in τ-(EDO-(S,S)-DMEDT-TTF)$_2$($AuBr_2$)($AuBr_2$)$_y$, it is likely that the Drude response is weak and/or very narrow, reminiscent of the low frequency response in β''-$(ET)_2SF_5CH_2CF_2SO_3$.[31] In that case, the total sum rule would be modified with another oscillator (quasiparticle band), however the partial sum rule should be still valid, with the reasonable estimation of m^*; as mentioned previously, the ionic conductivity may also make a partial contribution here. Considering different correlated pictures, one should remember that the specific 2D crystal structure of τ-(EDO-(S,S)-DMEDT-TTF)$_2$($AuBr_2$)($AuBr_2$)$_y$ (Fig. 1) differs from the quasi-one-dimensional architecture of prototype organic materials often discussed as applications. Therefore, the application of these models to experimental systems is not straightforward.

B. Vibrational properties

The vibrational features of τ-(EDO-(S,S)-DMEDT-TTF)$_2$($AuBr_2$)($AuBr_2$)$_y$ appearing in the MIR region are weak overall but well resolved in the ab plane conductivity spectrum and absorption spectrum taken in transmission mode (Fig. 5). The spectra do not show vibronic bands resulting from electron–phonon coupling of totally symmetric donor vibrations with the lowest electronic band,[36] as expected due to the low symmetry of the donor molecule. However, the temperature dependence in the range of the CH_2 stretching modes (inset, upper panel of Fig. 5) seems to be noticeably different for two specific modes; bands centered at ≈ 2860 and $2945\,cm^{-1}$ are much stronger and narrower at low temperature, respectively. Taking into account the presence of disorder in the hexagons containing two oxygens[37] and short S$\cdots$O contacts, the appearance of these modes can reflect small changes in the pattern of disorder in the conducting (ab) layer, influencing the interactions between organic molecules. The light CH_2-related endgroups of the organic building block molecular would naturally be most sensitive to such an interaction. This can serve as a mechanism for a disorder-driven localization at low temperature. Nevertheless, the effect is overall rather small in agreement with no structural change at low temperature.[17]

V. CONCLUSION

We report the optical properties of τ-(EDO-(S,S)-DMEDT-TTF)$_2$($AuBr_2$)($AuBr_2$)$_y$ salt ($y \approx 0.75$) as a function of temperature. This material seems to be in a charge-ordered state at 300 K. Unlike most other two-dimensional organic conductors, the low-lying electronic excitation develops an increasingly pronounced doublet structure with decreasing temperature. Fitting results reveal marked trends in the oscillator strength and center frequency of the narrow/low-frequency and broader/high-frequency components of the doublet structure. These trends suggest that the strong temperature dependence of this excitation is due to electronic localization. This localization may steal oscillator strength from a narrow, low-frequency Drude component. Some vibrational features in the range of CH_2 stretching modes also seem to be connected with the presence of low-temperature charge localization and disorder.

ACKNOWLEDGMENTS

I.O. and J.L.M gratefully acknowledge the National Science Foundation and North Atlantic Treaty Organization for support of this project (DGE 9804462). The Poznań/Athens collaboration is supported by the North Atlantic Treaty Organization under Collaborative Research Grant (HTECH CRG 972011). The authors thank Dr. M. Kubicki for technical assistance.

*Permanent address: Institute of Molecular Physics, Polish Academy of Sciences, Smoluchowskiego 17, Poznań, Poland.

[1] J.M. Williams, J.R. Ferraro, K.D. Carlson, U. Geiser, H.H. Wang, A.M. Kini, and M.H. Whangbo, *Organic Superconductors* (Prentice-Hall, Englewood Cliffs, NJ, 1992).

[2] O. Kahn, *Molecular Magnetism* (VCH, New York, 1993).

[3] A. Graja and O.A. Dyachenko, Macromol. Symp. **104**, 223 (1996).

[4] M. Kurmoo, A.W. Graham, P. Day, S.J. Coles, M.B. Hursthouse, J.L. Caulfield, J. Singleton, F.L. Pratt, W. Hayes, L. Ducasse, and P. Guionneau, J. Am. Chem. Soc. **117**, 12 209 (1995).

[5] P. Day, Mol. Cryst. Liq. Cryst. **305**, 533 (1997).

[6] J.A. Schlueter, K.D. Carlson, U. Geiser, H.H. Wang, J.M. Williams, W.-K. Kwok, J.A. Fendrich, U. Welp, P.M. Keane, J.D. Dudek, A.S. Komosa, D. Naumann, T. Roy, J.E. Schirber, W.R. Bayless, and B. Dodrill, Physica C **233**, 379 (1994).

[7] E. Coronado, J.R. Galan-Mascaros, C. Gimenez-Saiz, and C.J. Gomez-Garcia, Adv. Mater. Opt. Electron. **8**, 61 (1998).
[8] E.I. Zhilyaeva, O.A. Bogdanova, R.N. Lyubovskaya, R.B. Lyubovskii, K.A. Lyssenko, and M.Yu. Antipin, Synth. Met. **99**, 169 (1999).
[9] H. Urayama, H. Yamochi, G. Saito, K. Nozawa, T. Sugano, M. Kinoshita, S. Sato, K. Oshima, A. Kawamoto, and J. Tanaka, Chem. Lett. **1988**, 55 (1988).
[10] A.M. Kini, U. Geiser, H.H. Wang, K.D. Carlson, J.M. Williams, W.K. Kwok, K.G. Vandervoort, J.E. Thompson, D. Stupka, D. Jung, and M.-H. Whangbo, Inorg. Chem. **29**, 2555 (1990).
[11] J.M. Williams, A.M. Kini, H.H. Wang, K.D. Carlson, U. Geiser, L.K. Montgomery, G.J. Pyrka, D.M. Watkins, J.M. Kommers, S.J. Boryschuk, A.V. Strieby Crouch, W.K. Kwok, J.E. Schirber, D.L. Overmyer, D. Jung, and M.-H. Whangbo, Inorg. Chem. **29**, 3272 (1990).
[12] A. Terzis, A. Hountas, B. Hilti, G. Mayer, J.S. Zambounis, D.J. Lagouvardos, V. Kakoussis, G. Mousdid, and G.C. Papavassiliou, Synth. Met. **41–43**, 1715 (1991).
[13] G.C. Papavassiliou, D.J. Lagouvardos, A. Terzis, C.P. Raptopoulou, B. Hilti, W. Hofherr, J.S. Zambounis, G. Rihs, J. Pfeiffer, P. Delhaès, K. Murata, N.A. Fortune, and N. Shirakawa, Synth. Met. **70**, 787 (1995).
[14] J.S. Zambounis, J. Pfeiffer, G.C. Papavassiliou, D.J. Lagouvardos, A. Terzis, C.P. Raptopoulou, P. Delhaès, L. Ducasse, N.A. Fortune, and K. Murata, Solid State Commun. **95**, 211 (1995).
[15] K. Murata, N. Shirakawa, H. Yoshino, Y. Tsubaki, G.C. Papavassiliou, A. Terzis, and J.S. Zambounis, Synth. Met. **86**, 2021 (1997).
[16] G.C. Papavassiliou, D.J. Lagouvardos, J.S. Zambounis, A. Terzis, C.P. Raptopoulou, K. Murata, N. Shirakawa, L. Ducasse, and P. Delhaès, Mol. Cryst. Liq. Cryst. **285**, 83 (1996).
[17] K. Murata, H. Yoshino, Y. Tsubaki, and G.C. Papavassiliou, Synth. Met. **94**, 69 (1998).
[18] I. Olejniczak, W. Pukacki, and G.C. Papavassiliou, Adv. Mater. Opt. Electron. **6**, 288 (1996).
[19] N.A. Fortune, K. Murata, G.C. Papavassiliou, D.J. Lagouvardos, and J.S. Zambounis, Mater. Res. Soc. Symp. Proc. **328**, 307 (1994).
[20] G.C. Papavassiliou, D.J. Lagouvardos, I. Koutselas, K. Murata, A. Graja, I. Olejniczak, J.S. Zambounis, L. Ducasse, and J.P. Ulmet, Synth. Met. **86**, 2043 (1997).
[21] H. Yoshino, K. Iimura, T. Sasaki, A. Oda, G.C. Papavassiliou, and K. Murata, J. Phys. Soc. Jpn. **68**, 177 (1999).
[22] F. Wooten, *Optical Properties of Solids* (Academic, New York and London, 1972).
[23] C.S. Jacobsen, J.M. Williams, and H.H. Wang, Solid State Commun. **54**, 937 (1985).
[24] C.S. Jacobsen, D.B. Tanner, J.M. Williams, U. Geiser, and H.H. Wang, Phys. Rev. B **35**, 9605 (1987).
[25] H. Tajima, K. Yakushi, and H. Kuroda, Solid State Commun. **56**, 159 (1985).
[26] R. Świetlik and N.D. Kushch, Phys. Status Solidi A **142**, 515 (1994).
[27] R.H. McKenzie, Comments Condens. Matter Phys. **18**, 309 (1998).
[28] B.R. Bulka, *Proceedings of the 1998 Conference on Molecular Crystals, Gdańsk, Poland* [Mol. Phys. Rep. **25**, 41 (1999)]; LANL: cond-mat/9812392.
[29] S. Mazumdar, R.T. Clay, and D.K. Campbell, LANL: cond-mat/0003200.
[30] M. Dressel, A. Schwartz, G. Grüner, and L. Degiorgi, Phys. Rev. Lett. **77**, 398 (1996).
[31] J. Dong, J.L. Musfeldt, J.A. Schlueter, J.M. Williams, P.G. Nixon, R.W. Winter, and G.L. Ward, Phys. Rev. B **60**, 4342 (1999).
[32] M.J. Rozenberg, G. Kotliar, and H. Kajueter, Phys. Rev. B **54**, 8452 (1996).
[33] S. Mazumdar and Z.G. Soos, Phys. Rev. B **23**, 2810 (1981).
[34] K.C. Ung, S. Mazumdar, and D. Toussaint, Phys. Rev. Lett. **73**, 2603 (1994).
[35] P. Delhaes and C. Garrigou-Lagrange, Phase Transit. **13**, 87 (1988).
[36] V.M. Yartsev and A. Graja, Int. J. Mod. Phys. B **12**, 1643 (1998).
[37] C.P. Raptopoulou (private communication).